Cretaceous Research 72 (2017) 172–187

Contents lists available at ScienceDirect

Cretaceous Research

journal homepage: www.elsevier.com/locate/CretRes

Magnetostratigraphy of the Rabot Formation, Upper Cretaceous, James Ross Basin, Antarctic Peninsula

Florencia N. Milanese [a, *], Eduardo B. Olivero [b], Joseph L. Kirschvink [c, d], Augusto E. Rapalini [a]

[a] Universidad de Buenos Aires, Facultad de Ciencias Exactas y Naturales, Departamento de Cs. Geológicas, Instituto de Geociencias Básicas, Aplicadas y Ambientales de Buenos Aires (IGEBA-CONICET), Ciudad Universitaria, Intendente Güiraldes 2160, 1428 Buenos Aires, Argentina
[b] Centro Austral de Investigaciones Científicas (CADIC-CONICET), B. Houssay 200, 9140 Ushuaia, Tierra del Fuego, Argentina
[c] Division of Geological & Planetary Sciences, California Institute of Technology, Pasadena, CA 91125, USA
[d] Earth-Life Science Institute, Tokyo Institute of Technology, Meguro, Japan

ARTICLE INFO

Article history:
Received 14 January 2016
Received in revised form
22 December 2016
Accepted in revised form 27 December 2016
Available online 28 December 2016

Keywords:
Magnetostratigraphy
Antarctica
James Ross Basin
Upper Cretaceous
Paleomagnetism
Rabot Formation

ABSTRACT

Problems of endemism and diachronous extinctions make global correlation of coeval strata in the mid Campanian-Maastrichtian of the James Ross Basin problematic. To provide a more precise chronological framework, we present two magnetostratigraphies of Campanian strata from the Rabot Formation that crops out at Hamilton Norte (200 m thick) and Redonda Point (340 m thick) in James Ross Island. Sampled sections consist of poorly-consolidated, drab-colored fine sandstones and mudstones. Bulk susceptibility logs of both sections show a similar pattern of relatively low values at the lower and upper levels with significantly higher values at mid-levels that confirms the lithostratigraphic correlation between sections. Rock magnetic studies suggest that this change is not attributable to a ferrimagnetic fraction but to a paramagnetic contribution of presumed detrital origin. Stepwise thermal demagnetization showed dominant unblocking temperatures higher than 400 °C. Progressive hybrid low-temperature cycling, low-field AF and thermal demagnetization in a controlled N_2 atmosphere, reveals a two-polarity characteristic component of possible primary origin. Rock magnetic experiments suggest that detrital titano-magnetite is the most likely remanence carrier. Anisotropy of magnetic susceptibility results show sedimentary fabrics, indicating that beds were not significantly buried or compacted. Magnetostratigraphies produced at each locality demonstrate a consistent change from reverse to normal polarity remanence in the middle of the sections. Biostratigraphic constraints identify this reversal as the C33r/C33n transition, indicating a 79.90 Ma depositional age for this level of the Rabot Formation. The remanence directions yield a mean whose corresponding paleopole is consistent with two recently obtained Upper Cretaceous reference paleopoles for the Antarctic Peninsula. Our data support the lack of tectonic rotation or oroclinal bending of this region since the Late Cretaceous.

1. Introduction

The James Ross Basin (JRB), located at the northeastern tip of the Antarctic Peninsula (Fig. 1), comprises more than 6 km (del Valle et al., 1983) of marine sedimentary deposits Barremian to Eocene in age. Strata from James Ross Basin are of great scientific value because they preserve one of the most important, rich and continuous records of marine life for the Late Cretaceous in the Southern Hemisphere, also being of great importance for regional stratigraphic correlations (Feldmann and Woodburne, 1988; Reguero et al., 2013; Francis et al., 2016). The Cretaceous strata of the basin include the basal Gustav Group (Barremian-Coniacian), which corresponds to deep marine deposits (Ineson, 1989), and the Marambio Group (Santonian-Danian) which records deposition in transitional to platform environments (Macellari, 1988; Lirio et al., 1989; Medina et al., 1989; Pirrie et al., 1997; Whitham et al., 2006; Olivero et al., 2008; Olivero, 2012a).

Even though fossils are abundant, both the ammonites and palinomorphs present several global correlation problems due to their endemic distribution or diachronic extinctions patterns (Pirrie et al., 1997; Olivero, 2012a). The scarcity of suitable

* Corresponding author.
E-mail address: fnmilanese@gl.fcen.uba.ar (F.N. Milanese).

http://dx.doi.org/10.1016/j.cretres.2016.12.016
0195-6671/

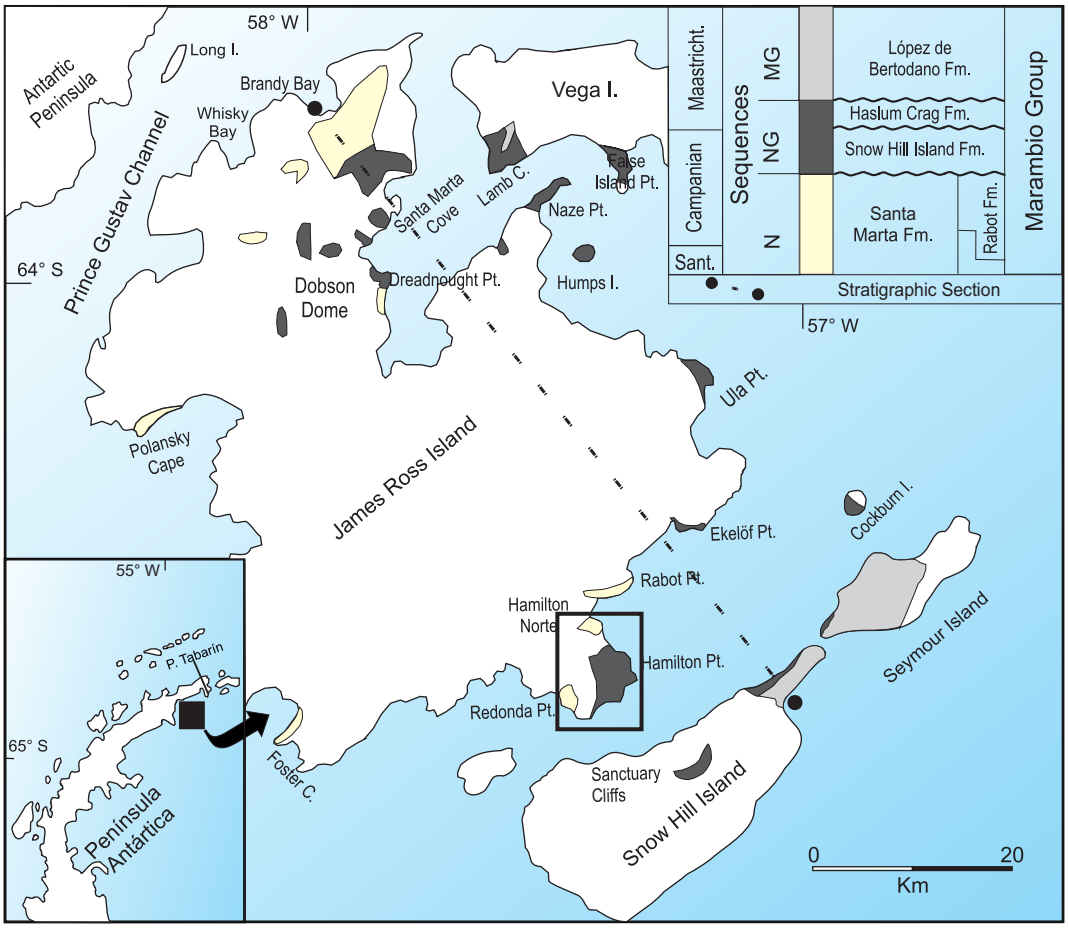

Fig. 1. Upper Cretaceous Marambio Group in James Ross archipelago. Black box shows the study area detailed in Fig. 3 (modified from Olivero, 2012a).

material for Ar/Ar or U/Pb dating makes magnetostratigraphy a valuable tool to provide a precise chronological framework for biostratigraphic, paleogeographic and paleoclimatic studies in the Antarctic Peninsula. Furthermore, magnetostratigraphy allows to compute sediment accumulation rates that provide significant information on the tectonic, paleoenvironmental, and climatic setting. In parallel, paleomagnetic pole positions provide paleolatitude constraints on the development of the basin fill and on major tectonic processes like crustal block rotation and oroclinal bending. Preliminary results obtained on the SE sector of JRB (Milanese et al., 2013) and previous work carried out on Seymour Island by Tobin et al. (2012) are an encouraging precedent for further paleomagnetic research on rocks of the JRB. This study is focused on two partial sections of the Rabot Formation exposed in Hamilton Norte (*HN*) and Redonda Point (*Re*) in southeastern James Ross Island (Fig. 1).

2. Geological framework

The James Ross Basin is interpreted as a back-arc basin developed to the east of a magmatic arc located along the Antarctic Peninsula. The arc was formed by the southeastward subduction of the proto-Pacific oceanic plate beneath the southern margin of Gondwana (Whitham, 1993; Hathway et al., 2000), with volcanism starting ~180 Ma ago. The JRB experienced continuous subsidence, providing the accommodation space for the deposition of more than 6 km (del Valle et al., 1983) of highly fossiliferous marine, deltaic and estuarine sediments from Barremian to Late Eocene time (Andersson, 1906; Rinaldi et al., 1978; Farquharson, 1984; Ineson et al., 1986; Olivero et al., 1986, 2008; Crame et al., 1991; Riding et al., 1998; Marenssi et al., 2002; Olivero, 2012a).

Our study was carried out on the Santonian-Danian Marambio Group (Rinaldi et al., 1978; Macellari, 1986; Olivero et al., 1986), which comprises 3 km of alternating mud, fine-grained sandstones and subordinated conglomerates and coquinas that have been interpreted as prograding deltaic lobes or platform deposits (Olivero et al., 1986, 2008; Pirrie, 1989; Crame et al., 1991; Pirrie et al., 1997; Olivero, 2012a) developed during a tectonic inversion stage of the basin (Ineson, 1989; Buatois and Lopez Angriman, 1992; Whitham et al., 2006).

Several different stratigraphies have been published for the Marambio Group (Fig. 2). In this work we follow the nomenclature proposed by Olivero (2012a). The Rabot Formation, exposed in the SE sector of the James Ross Island, is approximately equivalent to the Beta Member of the Santa Marta Formation (Olivero et al., 1986) exposed in the NW sector of the island. Proximal facies of the basin are located to the western sector while distal facies are represented by outcrops located to the East.

The Rabot Formation (Lirio et al., 1989) is well exposed in the type section at Rabot Point, as well as in Hamilton Norte and Redonda Point (Fig. 1). It is composed of members I, II and III (Lirio et al., 1989) or by the approximately equivalents units a, b and c according to Pirrie et al. (1997). This unit consists of an intercalation of mud, sandstones, tuffs and minor conglomerates. It represents

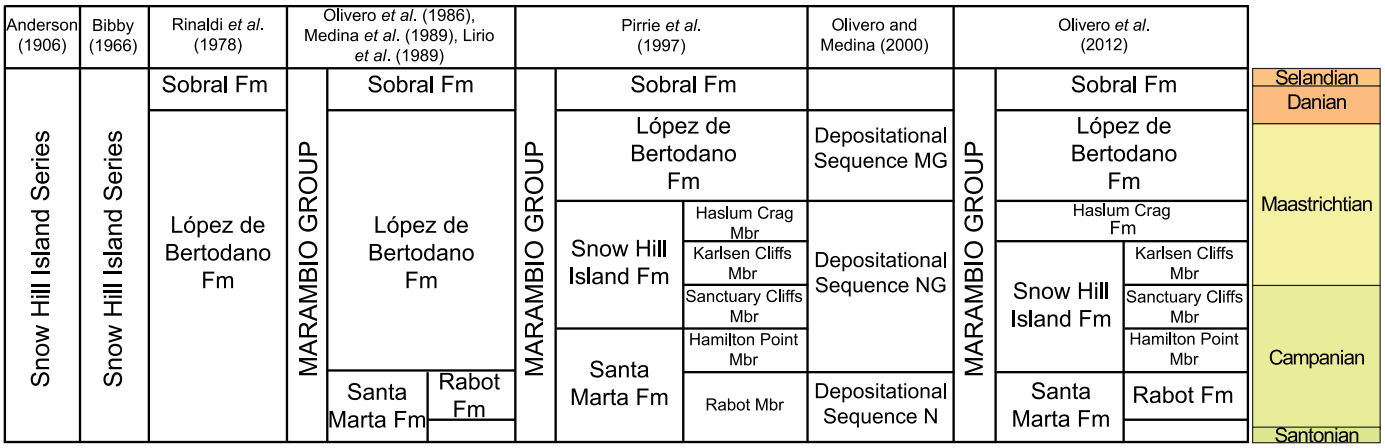

Fig. 2. Stratigraphic summary of Santonian-Danian Marambio Group (Bibby, 1966).

distal facies of a regressive sequence of a storm-dominated platform (Lirio et al., 1989), while proximal facies are represented by the Santa Marta Formation in the western side of the basin (Olivero, 2012a-b).

Based on main limiting unconformities, Olivero and Medina (2000) have defined the Depositional Sequence N (whose name is given by the genus *Natalites*, the most abundant kossmaticeratid ammonite) that encompasses the Santa Marta and part of the Rabot formations (Figs. 1 and 2). Macro and microfossils content (Lirio et al., 1989; Marenssi et al., 1992; Palamarczuk, 1993; Olivero, 2012a-b) indicates an early-middle Campanian age for the Rabot Formation.

In the northwestern area of the James Ross Island, the Santa Marta Formation includes six successive ammonite assemblages of Santonian (Assemblage 1) to early Campanian (Assemblages 2–6) age (Olivero, 1992). The strata preserving the uppermost Ammonite Assemblage 6 are erosively cut by the unconformity that separates the Santa Marta Formation from the overlying Snow Hill Island Formation. The basal conglomerate of the later formation preserves reworked diagnostic mid-Campanian ammonites, *Baculites Subanceps* Haughton, *Metaplacenticeras subtilistriatum* (Jimbo), *Hoplitoplacenticeras* sp., and *Neokossmaticeras redondensis* Olivero (Olivero, 2012b). In southeastern James Ross Island, these age-diagnostic ammonites are also recorded at the upper part of the Rabot Formation in Rabot Point, Redonda Point, and Hamilton Norte, where they characterize the Ammonite Assemblage 7. The later assemblage conformably overlies strata of the Rabot Formation preserving the early Campanian Ammonite Assemblage 6, implying that coeval strata were formed in northwestern James Ross Island, but they were eroded and the reworked fauna incorporated in the basal Snow Hill Island Formation (Olivero and Medina, 2000; Olivero, 2012a-b).

3. Methodology

One hundred and forty-five cylindrical cores of 2.54 cm in diameter were collected with a gasoline-powered drill during the Antarctic field seasons of February–March of 2010 (*HN*, from Hamilton Norte) and 2011 (*Re*, from Redonda Point). The first section is 210 m thick and the latter 330 m thick. A Pomeroy® orientor was used to orient the cores *in situ*.

HN and *Re* are located in the SE sector of James Ross Island and separated some 7 km from each other (Fig. 3). They include informal members b and c from Pirrie et al. (1997) and are approximate equivalents to members II and III of the Rabot Formation according to Lirio et al. (1989).

Although lithology of both sections is mostly unconsolidated mud, *in situ* paleomagnetic samples were taken on sandstone beds and spherical concretions. In addition, consolidated yellow tuff beds were found in the *Re* section. A prominent volcaniclastic sandstone bed, of characteristic green (in the web version) color due to its high content in glauconite, is present in both sections and is a very useful correlation tool in the field (Fig. 4).

In order to characterize the petrofabric, anisotropy of magnetic susceptibility (AMS) studies were carried out on all samples, using a Kappabridge™ multi-function susceptibilitimeter MFK1 on standard 11 cm^3 specimens. Low (−200 to 20 °C) and high (0–700 °C) temperature thermomagnetic curves were made with the same equipment. High temperature curves were realized in Ar atmosphere.

Hysteresis cycles were obtained for samples from *HN* section with a Molspin vibrating sample magnetometer (H_{max} = 1000 mT) at the Laboratorio de Paleomagnetismo Daniel A. Valencio of the IGEBA (University of Buenos Aires-Conicet, Argentina). An extra group of Rabot Formation samples, proceeding from Rabot Point locality (Fig. 1) were processed with a LakeShore 7404 magnetometer (H_{max} = 2000 mT) at the Laboratorio de Magnetismo of the Instituto de Física de La Plata (University of La Plata, Argentina).

Demagnetization was carried out at the Paleomagnetics and Biomagnetics laboratory of the California Institute of Technology, using an automatic 3-axis DC-SQUID moment magnetometer system, housed in a magnetically shielded room on 5.5 cm^3 specimens, following the general protocol developed for sediments of the James Ross Basin described by Tobin et al. (2012). The demagnetization routine started with two low-temperature cycling steps (samples were cooled to 77 K in liquid N_2 in a low-field space) to remove viscous magnetizations carried by multi-domain magnetite, followed by three low-intensity alternating field (AF) steps (from 2.3 to 6.9 mT) to remove secondary magnetizations acquired during collection and transportation of samples. Main demagnetization process was thermal, from 60 °C reaching up to 575 °C in 15–10 °C steps, with samples being demagnetized in a trickle of N_2 gas above 120 °C to minimize oxidation. Most samples showed unstable behavior above ~400 °C.

In ambiguous cases (e. g., samples of the same level with opposite polarities) stepwise AF demagnetization (up to 70 mT) was carried out to provide further information.

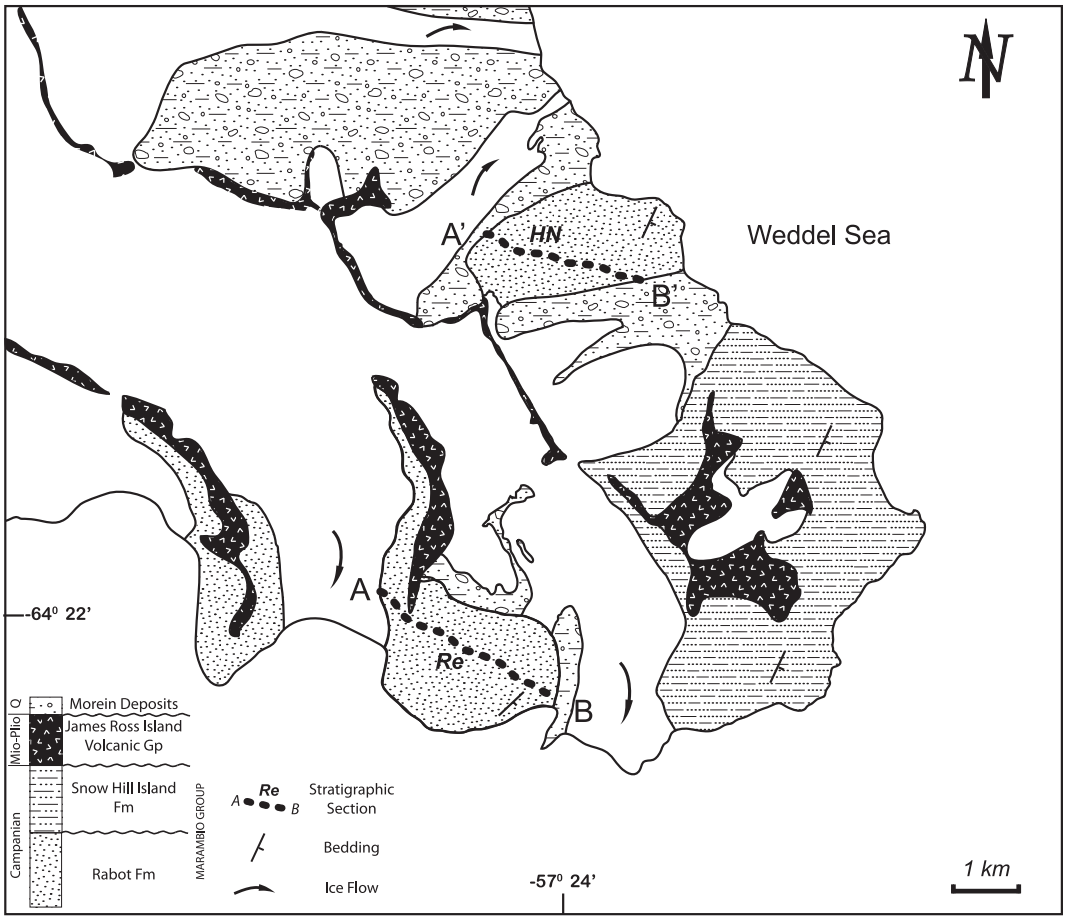

Fig. 3. Geological sketch of the study area. *HN* and *Re* section traces in dashed lines.

4. Results

4.1. Bulk susceptibility (k) and AMS

Average bulk susceptibility values for each stratigraphic level are shown in Fig. 4. Three bulk susceptibility domains are identified in both stratigraphic columns.

The same trend is identified in both *HN* and *Re*: a basal domain with relatively low *k* from the base of both sections up to around 70 m (*HN*) and 120 m (*Re*). This is followed by an interval of higher and more variable values of *k* extending from 70 m to 120 m (*HN*) and 120 m–225 m (*Re*) approximately. The glauconitic guide level is in this interval in both sections. The uppermost part of both sampled successions is again characterized by low and more uniform bulk susceptibility values, very similar to the lowest domain. Mean values with corresponding standard deviations for all domains of each section are shown in Table 1. The similar pattern of *k* in both sections probably reflects subtle changes in the parental material and sedimentation processes. In *Re* the central domain with higher *k* approximately correlates with an increase of sandstone beds in the succession. However, that does not seem to be the case in the *HN* section (Fig. 4).

Anisotropy degree (P_j) and bulk susceptibility values (K_m) are low at both localities (Figs. 5*A*, *B*). K_m and P_j are slightly higher in *HN* section with most samples showing values less than 10^{-4} SI and 1.05, respectively. Mean P_j are identical, 1.024 ± 0.014 and 1.023 ± 0.012 for *HN* and *Re* respectively. Shape parameter *T* (Jelinek, 1981) shows no clear correlation with *k*, and, although oblate shapes dominate, prolate ones are also observed, mainly associated with scarce cases of inverse fabrics (Figs. 5*C*, *D*, and 6). Anisotropy of low field Magnetic Susceptibility (AMS) stereographic diagrams for both sections are shown in Fig. 6. They show similar AMS character. Minimum susceptibility axes (*k3*) are orthogonal to the bedding plane (more pronounced in *Re*) while *k1* and *k2* are distributed along it. These are typical sedimentary or compactional fabrics. Redonda Point section, however, shows a subtle preferential orientation of maximum susceptibility axes (*k1*) in a NNE-SSW direction (Fig. 6) which is near orthogonal to principal paleocurrents directions of the Rabot Formation, of dominant ESE or ENE trends (Martinioni and Rinaldi, 1992; Olivero and Mussel, 1993). We discuss two possible explanations for this grouping later. Mean statistical values for maximun (*k1*), intermediate (*k2*) and minimun (*k3*) susceptibility axes for both sections are presented in Table 2.

Scarce samples from a consolidated tuffaceos level located at ~60 m from the bottom of the *Re* section show inverse fabric (Fig. 6). Samples from this group show prolate fabrics, which oppose the clear dominance of oblate fabrics along the whole succession (Fig. 5*D*).

4.2. Rock magnetism

Several rock magnetism studies as thermomagnetic curves, histeresys cycles, and Lowrie-Füller tests were carried out in order to determine the magnetic mineralogy. Studies were performed in samples with stable behavior during demagnetization.

Because sediments from *HN* and *Re* were deposited in a transitional-deep marine environment, greigite presence is likely.

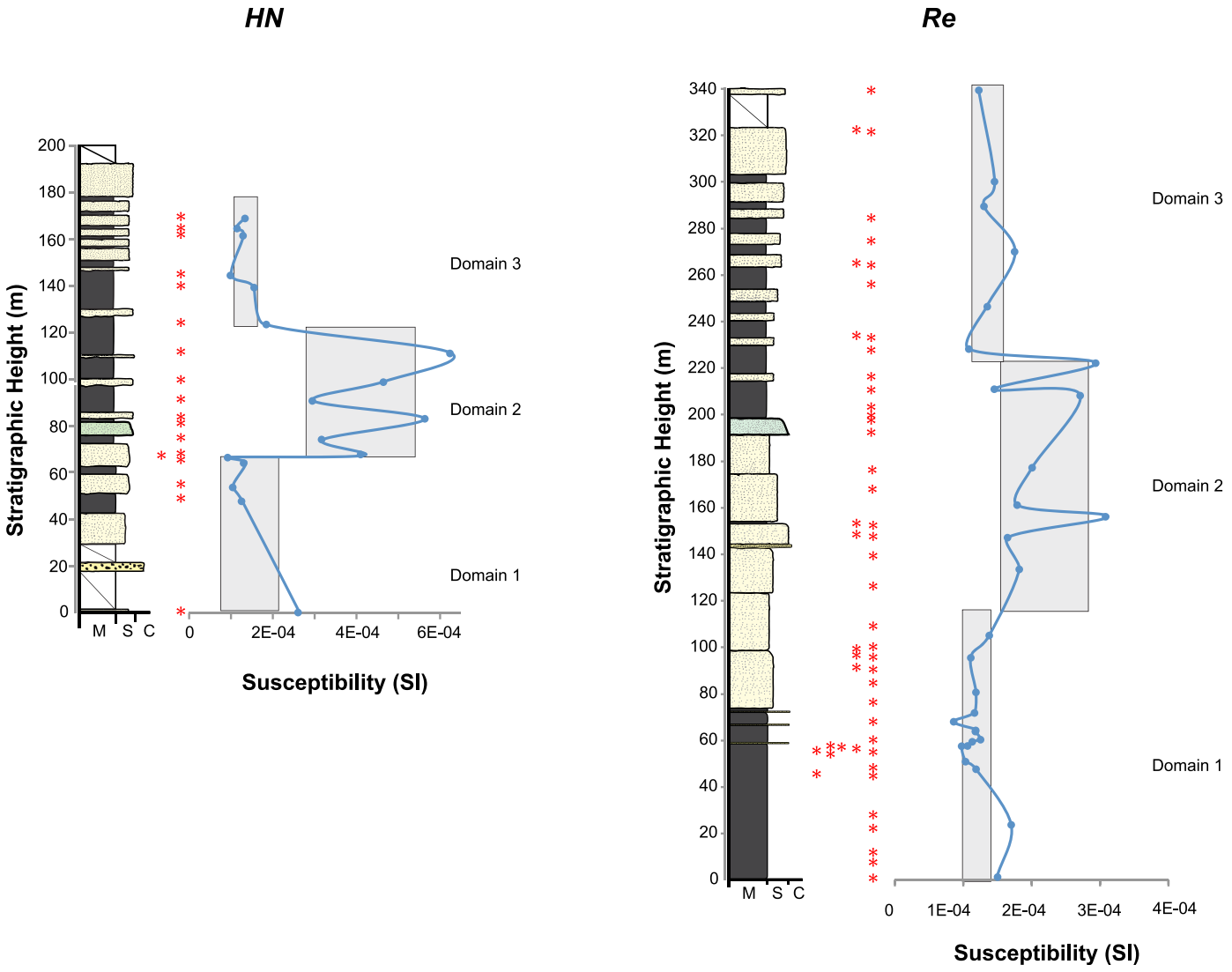

Fig. 4. Sedimentary logs, sampled levels (asterisks) and bulk susceptibility values from *HN* and *Re* localities. The guide volcaniclastic sandstone is colored in green. Three main susceptibility domains are identified in both sections. Rectangles show standard deviations for each domain. (For interpretation of the references to color in this figure legend, the reader is referred to the web version of this article.)

Table 1
k_{mean} values for susceptibility domains in *HN* and *Re* sections.

	K_{mean} (SI)	
	HN	Re
Domain 1	1.45E-04 ± 6.89E-05	1.19E-04 ± 2.07E-05
Domain 2	4.09E-04 ± 1.3E-04	2.18E-04 ± 6.39E-05
Domain 3	1.35E-04 ± 2.78E-05	1.36E-04 ± 2.32E-05

Rotational remanent magnetization (RRM) studies and analysis of parameters as remanence coercivity (H_{cr}) and median destructive field (MDF_{RRM}) were accomplished in order to test greigite presence.

Some of these studies were carried out in extra samples from Rabot Point (Fig. 1) and are identified in graphics as *Ra16*.

4.2.1. Thermomagnetic curves and hysteresis cycles

4.2.1.1. Thermomagnetic curves. The exponential decrease of bulk susceptibility (k) observed in low-T thermomagnetic curves (Figs. 7A, B) indicate that k values are likely governed by paramagnetic minerals.

High-T curves (Figs. 7C, D) show irreversible behaviors attesting to new mineral formation, likely magnetite, from about 400 °C. These results explain the typical thermal demagnetization behavior of the natural remanent magnetization of most analyzed samples that generally became unstable above 400 °C. Lack of any drop in the heating curve below that temperature suggests that the original carrier of the remanence has a Curie temperature higher than 400 °C (Ti-magnetite?). New magnetite formation probably occurred due to the transformation of clay minerals during experimental heating (Pan et al., 2000).

4.2.1.2. Hysteresis cycles. After subtracting the paramagnetic contribution, hysteresis data show the ferromagnetic characteristics of sedimentary rocks from *HN* and *Ra16* (Fig. 8). Magnetic parameters could be computed and they are shown in Table 3. *Ra16* samples lack of precise stratigraphic height data but they include almost the whole section thickness. No significant change in the hysteresis magnetic parameters is observed along the section. This suggests that the ferromagnetic fraction is essentially constant. H_c values between 14 and 22 mT (with exception of two samples that

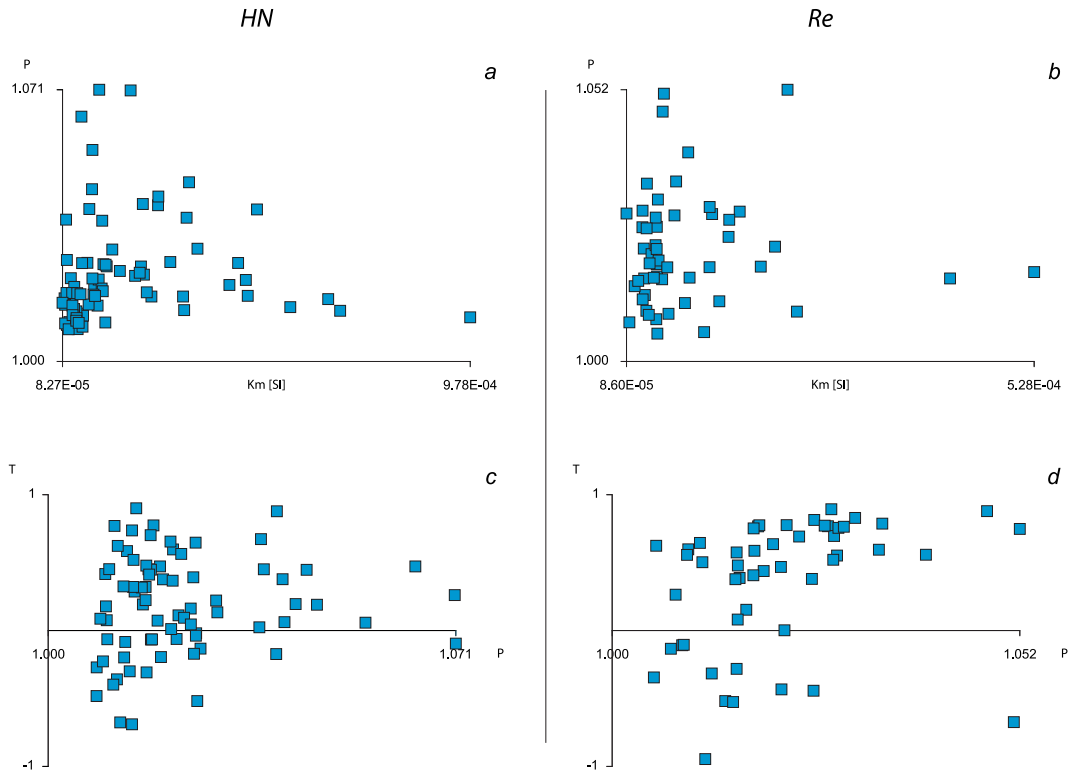

Fig. 5. Anisotropy degree P_j and susceptibility values (K_m) for *HN* (*A*) and *Re* (*B*) sections. Anisotropy degree *P* and shape parameter *T* for *HN* (*C*) and *Re* (*D*) sections.

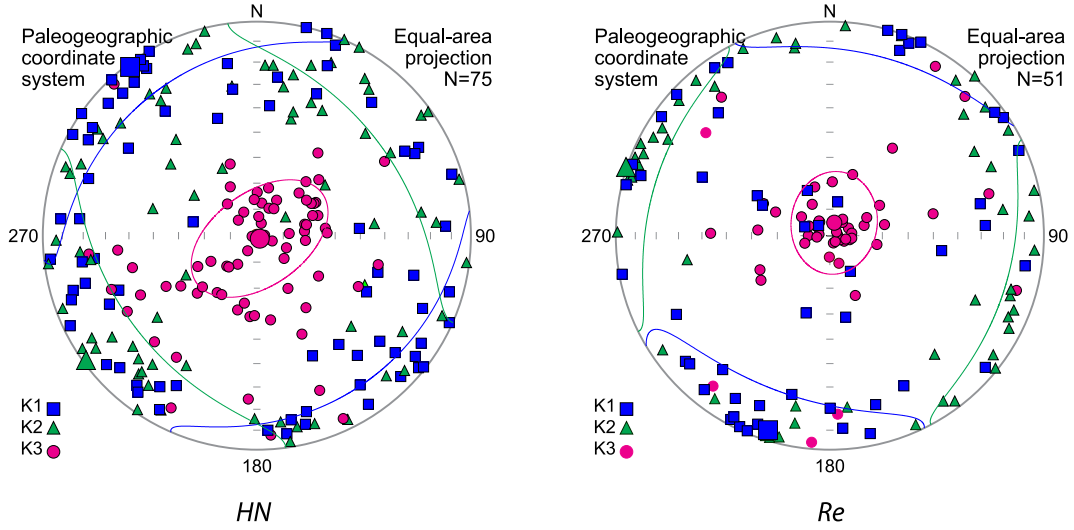

Fig. 6. AMS stereographic diagrams. Maximum (*k1*), intermediate (*k2*) and minimum (*k3*) susceptibility axes distribution of specimens from *HN* and *Re*. Bigger symbols correspond to the mean of AMS axes, which are presented with their 95% confidence ellipses. Plot is in bedding-corrected coordinates. Schmidt's net lower hemisphere projection.

Table 2
Mean tensor for *HN* and *Re* sections. E1 and E2 are the maximum and minimum axes of the 95% confidence ellipse around the mean direction.

HN section				Re section			
N = 75	Value	Dec/Inc (°)	E1/E2 (°)	N = 52	Value	Dec/Inc (°)	E1/E2 (°)
K1	1.005	323.1/1.6	60.9/17.4	K1	1.005	197.6/5.2	44.1/19.3
K2	1.003	233.1/0.2	60.8/29.4	K2	1.003	287.6/0.1	44.2/°15.9
K3	0.992	136.1/88.4	29.5/17.7	K3	0.992	18.6/84.8	19.6/16.3
K_m		**2.21E-04 ± 1.67E-04**		**K_m**		**1.53E-04 ± 8.10E-05**	

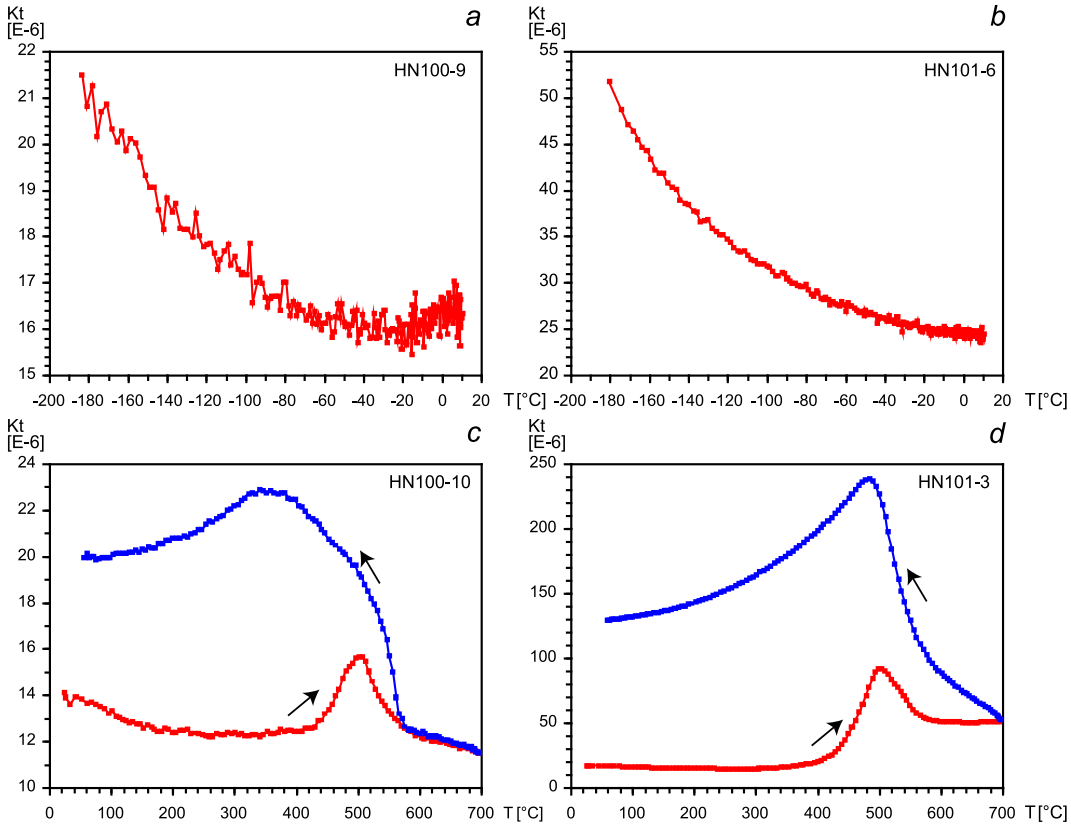

Fig. 7. Thermomagnetic curves for samples of *HN* section. Low temperature curves for samples of *Domain 1 (A)* and *Domain 3* (*B*). High temperature curves for samples of *Domain 1* (*C*) and *Domain 3* (*D*) where lower red curve is for heating and blue for cooling. (For interpretation of the references to color in this figure legend, the reader is referred to the web version of this article.)

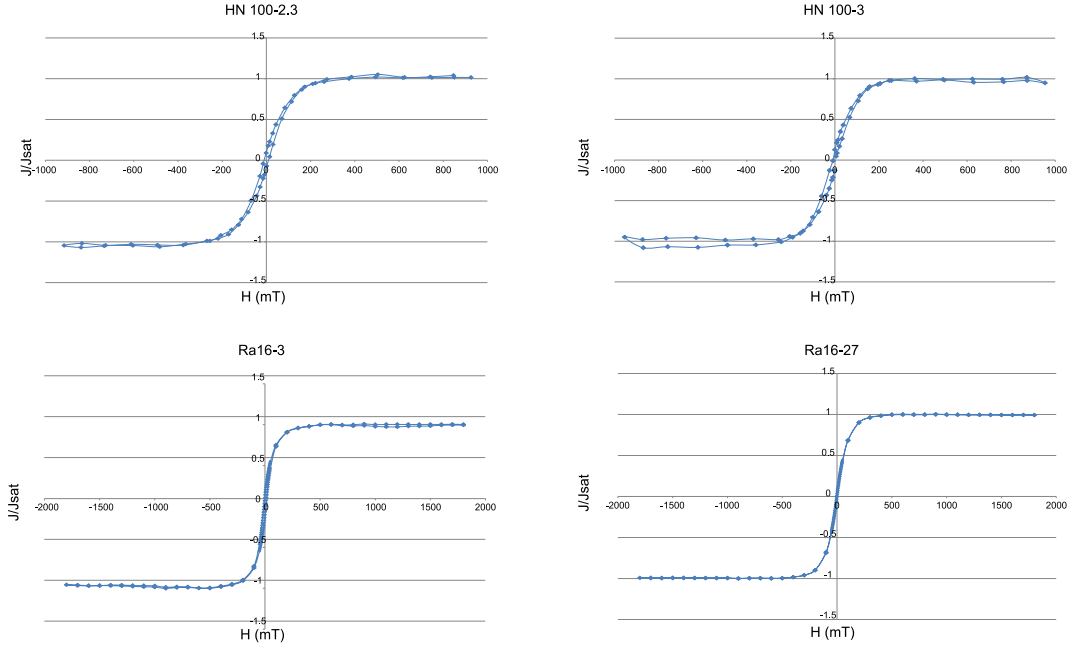

Fig. 8. Slope-corrected normalized hysteresis cycles. Two different VSM routines were used in samples from *HN* and *Ra16*. H_{sat} values are better determined in *HN*. J_r and H_c are more precisely calculated in *Ra16* due to major density of data in the central part of the cycle. HN100 samples correspond to *HN* section and Ra16 are samples from Rabot Formation, collected at Rabot Point locality (Fig. 1). See additional figures in Supplementary Data for extra hysteresis cycles examples.

Table 3
Parameters obtained from hysteresis cycles shown in Fig. 8. Two different VSM routines were used in samples from *HN* and *Ra*. H_{sat} values are more accurate in *HN*. J_r and H_c are more precisely calculated in *Ra16* due to major density of data in the central part of the cycle. HN100 samples correspond to *HN* section and *Ra16* are samples from Rabot Formation taken in Rabot Point locality (Fig. 1). Although stratigraphic level was not measured in this locality, they represent almost complete Rabot Formation thickness.

Sample	J_{sat} (A/m)	J_r (A/m)	H_c (mT)	H_{sat} (mT)
HN100-2.3	10.49	0.86	10.04	384.84
HN100-3	2.80	0.24	7.55	308.5
HN100-10.2	5.06	0.67	12.16	205.91
Ra16-3	9.81	1.11	9.49	500
Ra16-4	4.98	0.68	9.07	500
Ra 16-12	1.33	0.46	21.78	500
Ra16-19	1.94	0.31	13.91	500
Ra16-20	1.7	0.063	15.02	500
Ra16-26	23.83	0.89	3.72	400
Ra16-27	31.39	0.93	3.03	500
Ra16-42	7,14	1,25	18.66	500
Ra16-45	1,56	0,24	14.65	500

have anomalous H_c, probably due to MD presence) are consistent with a ferrimagnetic phase (Ti-magnetite?) as dominating the ferromagnetic signal. This is consistent with thermomagnetic data. Two different VSM routines were used, and *Ra16* samples have higher density of measurements than *HN* in the central part of the cycle (Fig. 8).

4.2.2. RRM, H_{cr} and MDF_{RRM}

Suzuki et al. (2006) show that greigite rotational remanent magnetization increases with the increment of rotation rate. Samples from Rabot Formation were put through a 90 mT field while increasing the spin frequency and no systematic increase nor notorious changes in RRM acquisition were observed in most of the samples (Fig. 9).

In Fig. 10, we compare Rabot Formation coercivity of remanece (H_{cr}) values with greigite H_{cr} values obtained by Roberts (1995). Two independent normal distributions are given by both studies and no significant overlap is observed, indicating that it is unlikely that greigite is the remanence carrier in samples from *HN* and *Re* sections. Values of H_{cr} from Rabot Formation samples are given in Table 4.

After rotating samples under a 100 mT field, Snowball (1997) computed median destructive fields (MDF_{RRM}) of the RRM acquired, that vary between 75 and 90 mT in greigite samples. MDF_{RRM} from four samples of Rabot Formation (Table 5) are between 25 and 50 mT, which are considerably lower than values given by of Snowball (1997) for greigite and consistent with values for magnetite (43–68 mT for SD).

4.2.3. Lowrie-Füller tests and Day Plot

Once greigite was ruled out and assuming Ti-magnetite as the likely carrier of the remanence, Lowrie-Füller tests (Lowrie and Fuller, 1971; Johnson et al., 1975) were carried out to define the dominant domain-state of the ferromagnetic fraction. Their results are shown in Fig. 11. In all samples anhysteretic remanent magnetization (ARM) was more resistant to AF demagnetization than isothermal remanent magnetization (IRM). This suggests that the remanence carriers are dominantly single domain or pseudo single domain.

Day et al. (1977) plot for samples from Rabot Formation is shown in Fig. 12. From a total of 9 samples, 2 fall in the MD zone, 5 in the PSD zone and the two remaining, in undetermined regions. The two MD field samples are Ra16-26 and Ra16-27, which present the

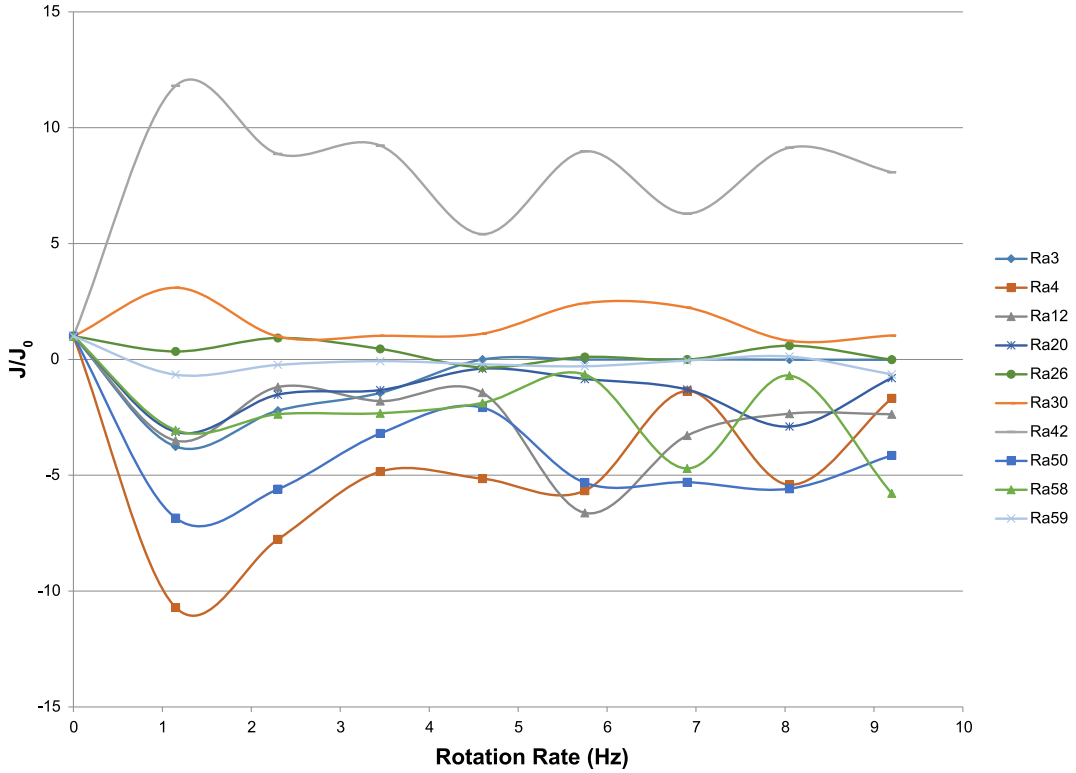

Fig. 9. Rotational remanent magnetization. No increase of magnetization is observed in samples of Rabot Formation with increase of the spinning frequency. J is normalized to each sample J_0 value, which varies from 1.84E-11 to 1.5E-9 Am^2.

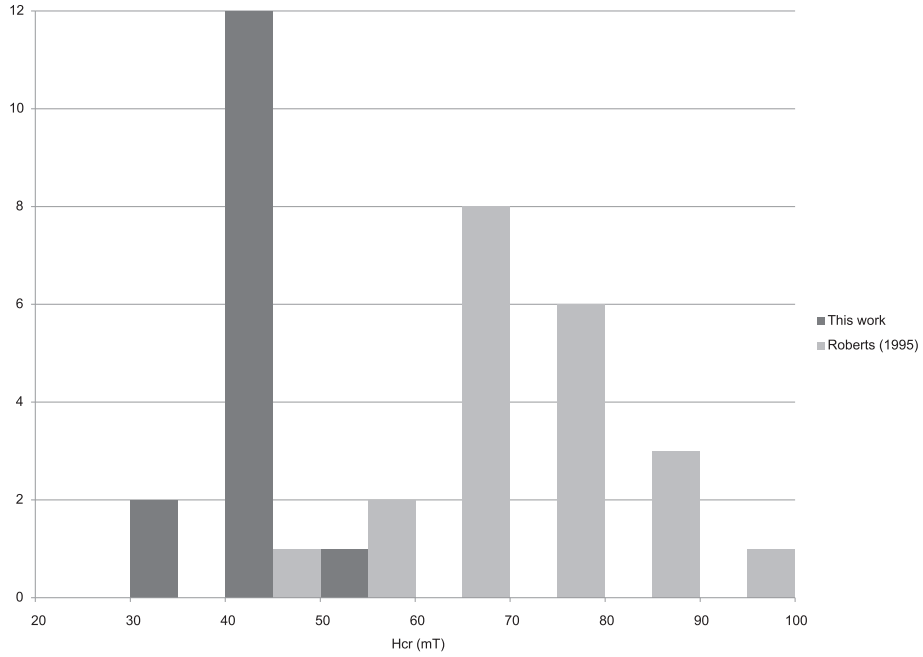

Fig. 10. Histogram comparing H_{cr} values for greigite (Roberts, 1995) with those from samples of the Rabot Formation. Note that both groups present significantly different H_{cr} values suggesting that greigite is not significant in the Rabot Formation. Values are given in Table 4.

lowest H_c values (~3 mT, see Table 3). According to Day et al. (1977) criteria, most remanence carriers from Rabot Formation are therefore pseudo-single domain.

4.3. Magnetostratigraphy

According to their demagnetization, samples showing stable remanence were used to build the magnetostratigraphy. Characteristic remanence (ChRM) directions were calculated by means of principal components analysis (PCA, Kirschvink, 1980). Only those with maximum angular deviation (MAD) values under 10° were accepted. In some cases, great circle analysis (McFadden and McElhinny, 1988) was performed to constrain the remanence direction along an arc. Most samples from which a ChRM could be computed had a single magnetic component, although in many cases a small viscous component was removed with the first steps of low-temperature demagnetization, AF or thermal cleaning up to 150 °C. A significant number of specimens, however, showed instability. Even in those with one univectorial direction, thermal demagnetization could not proceed further than 400 °C in most cases, due to a dominant viscous behavior produced by chemical changes upon heating.

From a total of one hundred and forty five independently oriented cores, we could isolate reliable directions from 60 of them. Examples of Zijderveld diagrams (Zijderveld, 1967) of samples with stable and unstable magnetization are illustrated in Fig. 13. Unstable samples were discarded from computing both the magnetostratigraphies and the mean direction. Most of the remaining samples presented stable behaviors until ~400 °C.

Both sections yielded similar magnetostratigraphies (Fig. 14), except for a normal polarity interval of ~10 m defined by three samples at the base of *Re*. Columns are characterized by a lower part of dominant reverse polarity and an upper part of dominant normal polarity, that presents a short reverse interval that can be correlated towards the top of both sections. Biostratigraphic data (Olivero and Medina, 2000; Olivero, 2012a, 2012b) indicate the lower part of sections *HN* and *Re*, including the Ammonite Assemblage 6, are of early Campanian age and the upper part of both sections, including the Ammonite Assemblage 7, are of mid Campanian (or basal late Campanian in the bipartite division of

Table 4
Coercivity remanence. Compared H_{cr} values of greigite from Roberts (1995) and from samples of Rabot Formation (this work).

Roberts (1995)	H_{cr} (mT)	Sample	H_{cr} (mT)
EJEM 07	80.6	Re55.5	49.1
EJEM 08	81.5	Re130.7	39.6
EJEM 09F	71	Ra3	41.3
EJEM 09I	68.4	Ra4	33.3
EJEM 09C	71.6	Ra12	47.4
EJEM 10F	67.5	Ra19	41.7
EJEM 10I	68.1	Ra20	40.1
EJEM 10C	63	Ra26	19.5
EJEM 11	81.7	Ra27	15.2
EJEM 12	68.3	Ra30	46.0
EJEM 13	62.8	Ra42	49.2
EJEM 14	71.2	Ra43	52.7
EJEM 15	68.9	Ra45	44.1
EJEM 16	77.4	Ra48	43.4
EJEB 375 + 376	77.5	Ra50	48.2
EJEB 380	94.8	Ra58	47.3
Krs	44.8	Ra59	44.4
Simpson	60.3		
Saddleback	70.2		
SYN90B	51.6		
SYN93A	58		

Table 5
MDF_{RRM} for Rabot Formation samples. Values between 25 and 50 mT are considerably lower than values given by of Snowball (1997) for greigite and consistent with values for magnetite.

Sample	MDF_{RRM} (mT)
Ra12	25.58
Ra19	49.38
Ra58	27.96
Ra59	26.91

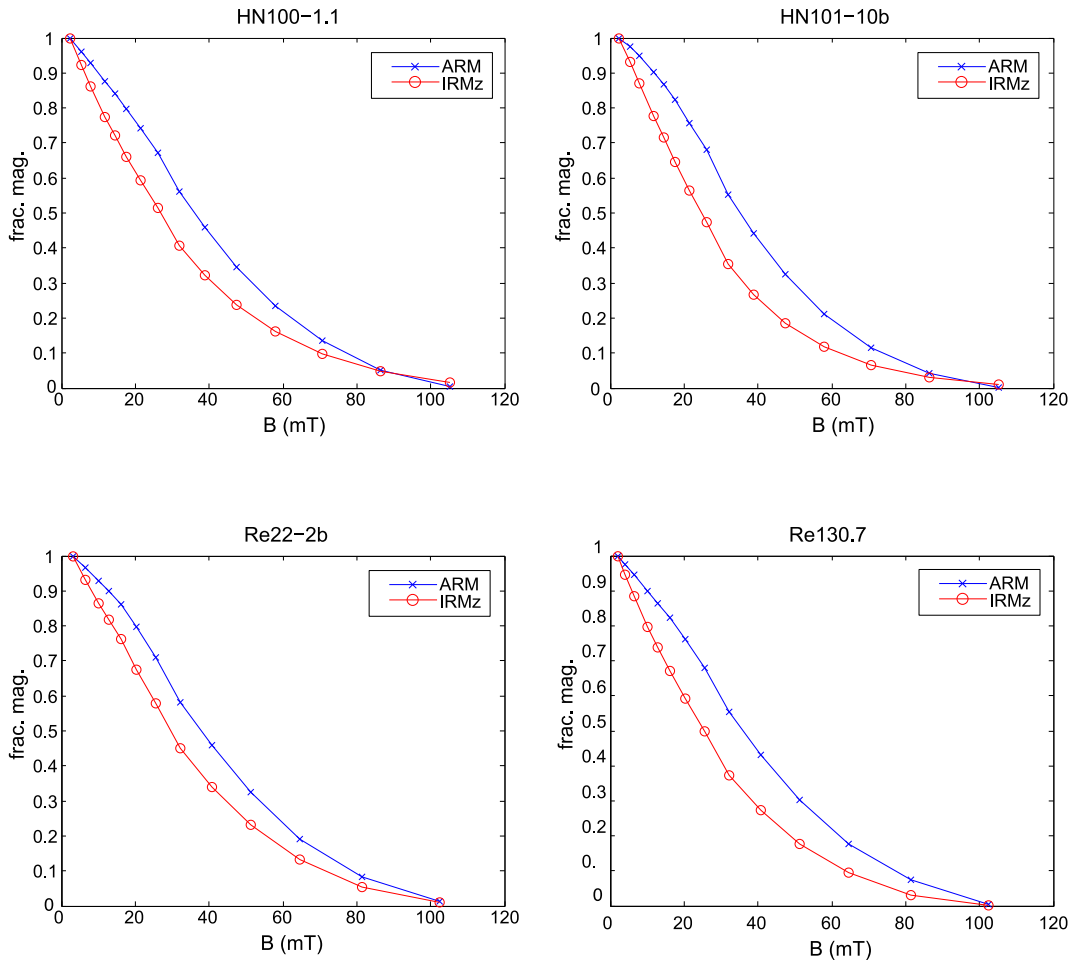

Fig. 11. Lowrie-Füller tests for samples from Domain 1 (*A*), 2 (*B*), and 3 (*C*) of *HN* section. See Suplementary Data for extra Lowrie-Füller test examples.

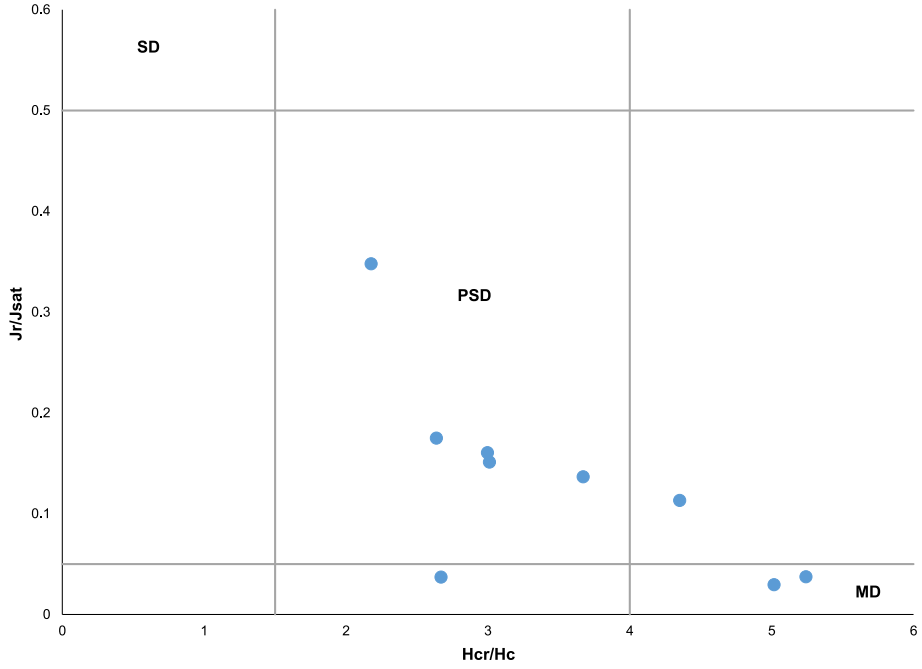

Fig. 12. Day et al. (1977) plot for samples of the Rabot Formation. Most of the samples fall in the PSD domain of the plot.

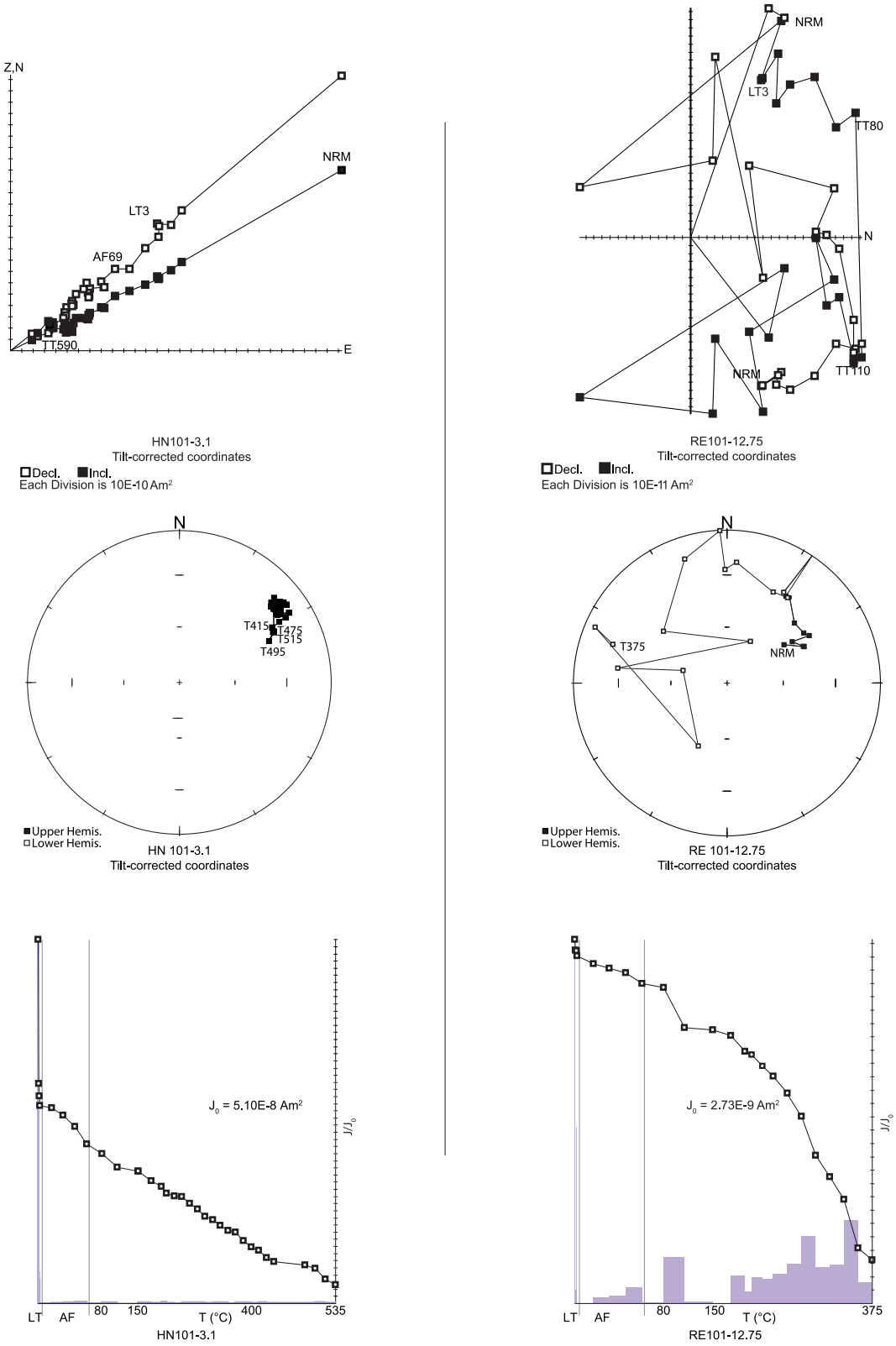

Fig. 13. Demagnetization behavior. Zidjerveld diagrams, stereoplots and J/J_0 plots for stable (left) and unstable (right) samples. Stable samples show straight decay to the origin and good direction grouping. Almost total remanence is eliminated before 400 °C; above that temperature, decay stops due to new magnetic mineral formation.

the Stage) age. Assemblage 6 is defined by the first appearance of *Karapadites* and last appearance of *Natalites*. Association 7 is defined by first appearance of *Neokossmaticeras redondensis* Olivero, which in the Rabot Formation is associated with *Metaplacenticeras subtilistriatum* and *Hoplitoplacenticeras* sp. Based on the biostratigraphic constraints, we interpret the local magnetostratigraphies and their correlations as shown in Fig. 15.

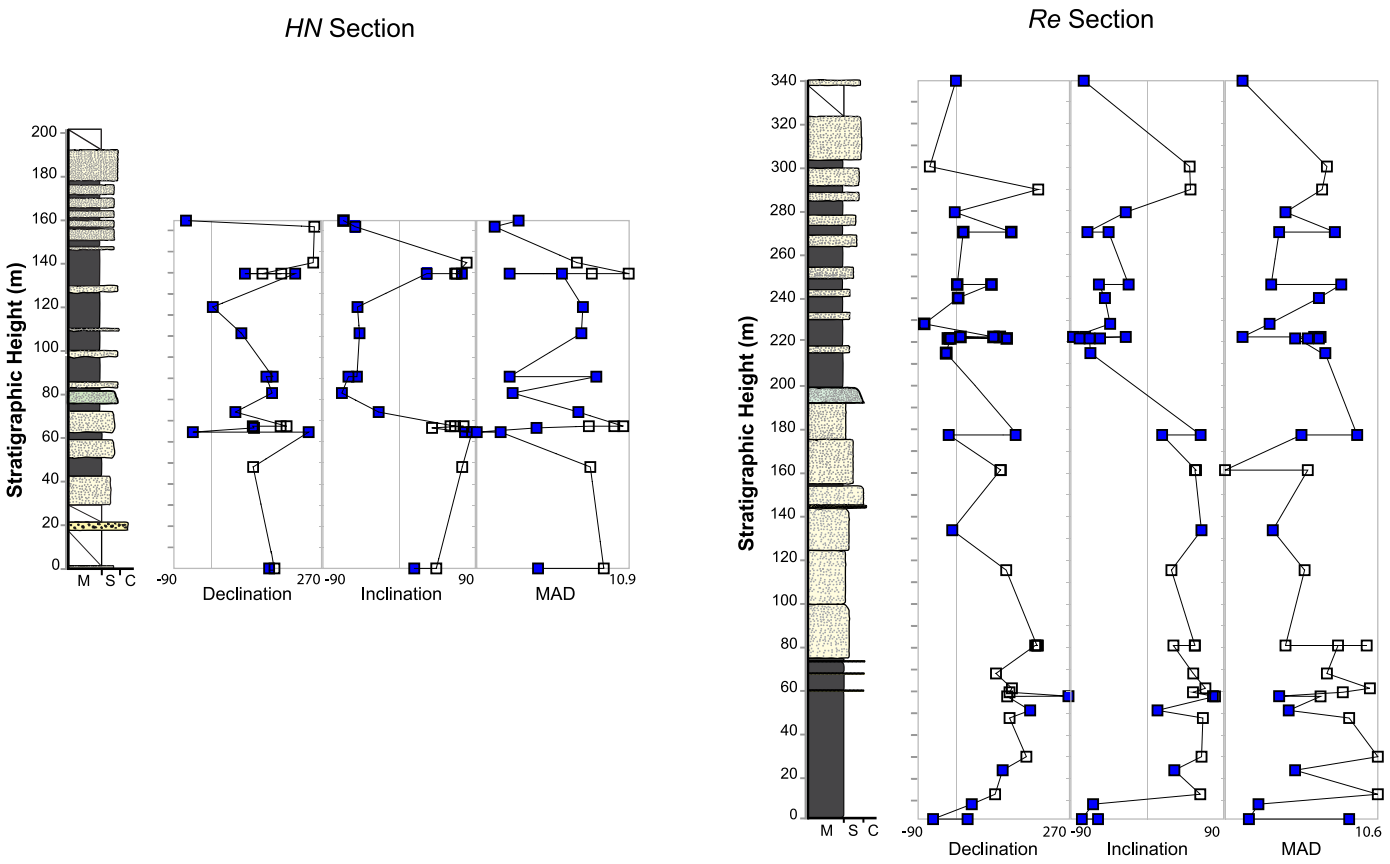

Fig. 14. Declination, Inclination and MAD for paleomagnetic directions of *HN* and *Re*. In solid squares, directions obtained from lineal regression by means of PCA (Kirschvink, 1980). In open squares, directions obtained from great circle analysis. Directions are in bedding-corrected coordinates.

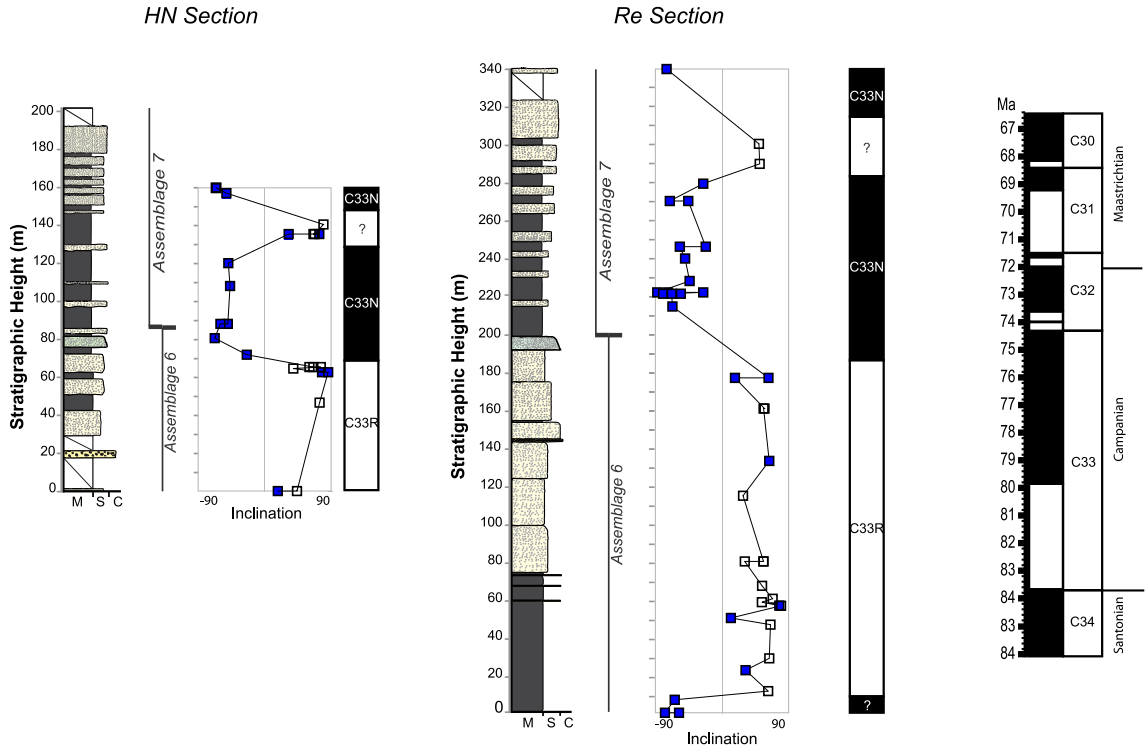

Fig. 15. Correlation of both magnetostratigraphies of the Rabot Formation with the Geomagnetic Polarity Time Scale of Gradstein et al. (2012). Both sections record the transition from C33r to C33n (79.90 Ma).

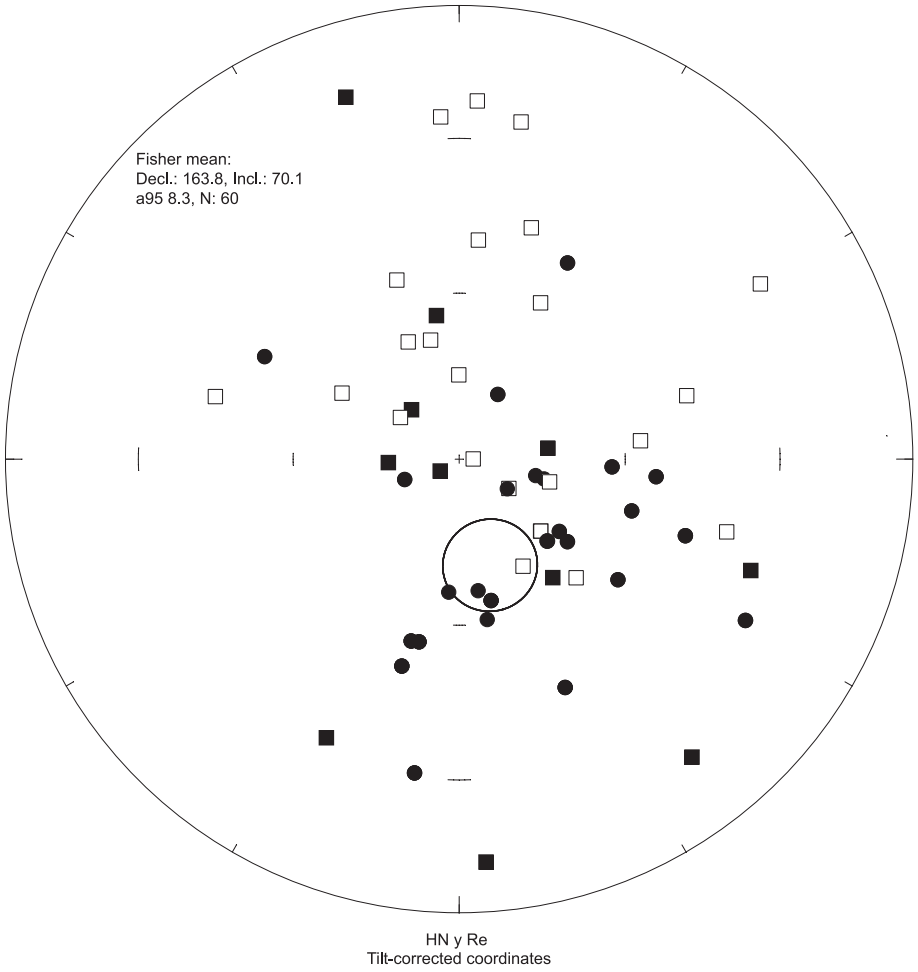

Fig. 16. Bedding corrected mean remanence direction for *HN* and *Re* given by Fisher statistics considering PCA and maximum circles. Normal directions were reversed for mean calculation. Solid (empty) symbols correspond to lower (upper) hemisphere projection. Squares are for directions obtained using PCA (Kirschvink, 1980) and circles for directions obtained from maximum circles (McFadden and McElhinny, 1988). Values are shown in Table 6. Because this distribution does not lead to a positive reversal test (McFadden and McElhinny, 1990), only PCA components were used to calculate the paleopole.

Only magnetostratigraphy data (ChRM components) were used to calculate the mean direction for samples from both sections. The tilt corrected value for this direction is **Dec:** 163.8°, **Inc:** 70.2°, **α95**: 8.2° and is shown in Fig. 16. Geographic and tilt corrected directions are given in Table 6. Tilt test results indeterminate and reversal test is negative (critical angle 16.3°, observed angle 18.2°). Selecting reverse directions obtained from PCA only (Table 6) results in a positive reversal test (critical angle 26.5°, observed angle 17.5°).

Table 6
Mean paleomagnetic directions from *HN* and *Re* sections. The first group of reverse directions lead to a negative reversal test and the second (PCA only) to a positive indeterminate reversal test (McFadden and McElhinny, 1990). Reversal tests were calculated using tilt corrected directions. Paleomagnetic pole was calculated using tilt corrected PCA directions only.

	Dec (°)	Inc (°)	α95	k	R	n
Geographic Mean Direction	192.5	78.8	8.21	5.81	51.5	62
Tilt Corrected Mean Direction	163.8	70.2	8.24	5.78	51.4	62
Tilt Corrected Normal Mean Direction	16.0	−70.0	12.6	6.2	21.2	25
Tilt Corrected Reverse Mean Direction	145	67.3	10.6	5.9	30.9	37
Tilt Corrected Reverse Mean Direction (PCA only)	139.2	73.3	28.6	2.9	8.6	12
Tilt Corrected Mean Direction (PCA only)	359.0	−68.8	11.8	4.8	29.5	37
Reversal test (All)	Critical Angle (°)		Observed Angle (°)		Condition	
	16.3		18.2		Negative	
Reversal test (PCA Only)	Critical Angle (°)		Observed Angle (°)		Condition	
	26.5		17.5		Positive (Indeterminate)	
	Lat	Long	Dp	Dm		
Paleopole (PCA only)	−77.9	119.7	31.4	26.6		

5. Discussion

Bulk susceptibility values along both successions allowed to define three subsections or susceptibility domains. Fig. 4 shows the correlation between these domains and the lithology logs. A prominent volcaniclastic glauconitic green bed is a conspicuous guide-level that occurs in the middle susceptibility domain of both sections, characterized by relatively higher values of bulk susceptibility. However, it is near the bottom of *Domain 2* at *HN* and near the top of the same domain at *Re*. Susceptibility values do not seem to correlate strictly with grain size or bed thickness. Whichever the source of this increase, it is apparent that it is somewhat diachronic, occurring first in the *Re* section (Fig. 4).

Both sections present sedimentary to low copactional magnetic fabrics with *k3* axes perpendicular to the bedding plane and *k1* and *k2* distributed along it. Maximun susceptibility axes (*k1)* present a subtle grouping in an almost perpendicular direction to paleocurrents trends in *Re* section (Fig. 6). This pattern can be assigned either to the result of orthogonal alignment of the longer axis of magnetic (and non magnetic) grains carried by traction (Ellwood and Ledbetter, 1977), or to a very weak tectonic overprint developed during the Late Cretaceous inversion of the James Ross Basin (Ineson, 1989; Buatois and López Angriman, 1992; Whitham et al., 2006). Several recent studies have shown that *k1* axes tend to align with the regional stretching direction in basins submitted to extensional regimes and perpendicular to the maximun regional stress in compressional regimes (Mattei et al., 1997; Sagnotti et al., 1999). A NNE regional stretching direction is consistent with the tectonic regional framework (main stress in NW-SE direction) during the Late Cretaceous compressional event. Small scale reverse faults affecting the Cretaceous strata have been identified in Rabot, Redonda and Hamilton points (Figs. 1 and 3). They support the interpretation for a mild compressional tectonic "cryptofabric" being represented by a *k1* grouping in *Re* section.

Scarce samples from a tuffaceous level in the lower section of *Re* show inverse magnetic fabric and present prolate AMS ellipsoids. In section 4.2, we characterized the remanence carrier for the study sediments as PSD titanomagnetite. Since PSD behavior can be the result of mixing of MD and SD grains, as demonstrated by Dunlop (2002), an inverse magnetic fabric at this level by dominance of SD titanomagnetite grains is a viable explanation, although it should be confirmed with more detailed rock-magnetic data at these specific levels.

Curie temperatures found in most samples are higher than 400 °C while saturation magnetic field (H_{sat}) are between 200 and 400 mT. These values suggest titanomagnetite as the most likely carrier of the remanence of these rocks. Several rock magnetism analyses, like RRM and comparison of magnetic parameters (H_{cr} and MDF_{RRM}) ruled out the presence of greigite. Lowrie-Fuller tests and Day Plot indicate pseudo-single domain grains as the remanence carriers. Magnetic fabric results clearly show a sedimentary fabric with a low compaction degree, consistent with a primary remanence, despite the fact that the tilt test results are indeterminate due to the homoclinal character and low degree of tilting of the strata.

Magnetic polarities could be consistently assigned to both sections, and indicate a lower section of reversed polarity followed by an upper section with dominant normal polarity, with the interpretation of having the C34N/C33R boundary at the base of the *Re* section. The age and correlation of the magnetic columns were constrained from ammonite assemblages according to Olivero (2012a-b), who assigned an early - middle Campanian age to the sections. Correlation with the Global Polarity Time Scale from Gradstein et al. (2012) strongly indicates that both sections record the transition from C33r to C33n (79.90 Ma, Fig. 15). This is located at 71 m in *HN* and at 195 m in *Re*. However, in the latter, the polarity transition occurs in a stratigraphic gap of nearly 40 m, and it could be preliminary assigned midway between last reverse level at 177 m and first normal level at 215 m. In *HN*, the C33r/C33n transition is precisely located 10 m below the glauconitic volcaniclastic green guide bed (located at 84 m). Allowing for the uncertainty in the *Re* section, we preferred to assign this transition in this section at the same stratigraphic distance below that guide-level located at 198 m.

At the bottom of *Re* we found normal polarity along the first 15 m. In According to the GPTS, it could correspond to the end of the Cretaceous Normal Superchron C34. However, this would contradict pre-existing biostratigraphic constraints. In this interval, the ammonites are the same as those recorded in the late early Campanian Ammonite Assemblage 6 of the Santa Marta Formation (Olivero, 2012a). In addition, typical Santonian ammonites, like those of the Ammonite Assemblage 1 in the Santa Marta Formation, including *Eubostrychoceras elongatum* (Whiteaves), *Polyptychoceras obstrictum* (Jimbo) and *Baculites kirki* Matsumoto, are not found in the lower part of the Rabot Formation. Moreover, preliminary, yet unpublished, magnetostratigraphic results from Santa Marta Formation show the C34n/C33r boundary located on top of the Santonian Ammonite Assemblage 1, and lying several hundred meters below the stratigraphic levels carrying the ammonites assemblages found in *Re* and *HN* sections.

Discarding the presence of C34N in the studied sections, there are two possible explanations for this normal interval. First, the presence of secondary components masking the ChRM; second, the presence of a brief normal interval or excursion at the base of C33r, as the ones found by Montgomery et al. (1998) in chalk successions of Southern England for the same time age. Just three samples define this normal interval; they present a stability range up to 235–390 °C and one of them decay straight to the origin. The other two show a normal stable cluster of directions that remains stable until new magnetic mineral formation provokes confusing demagnetization behaviors. Despite the fact that this brief interval has been found in just one of the sections, we consider the second possibility more likely, as no particularly different magnetic behavior was found in these samples from those of reverse polarity immediately up the section (see Supplementary Data).

This correlation gives an age of 79.90 Ma for middle levels of the Rabot Formation, which is the established age for C33r/C33n transition (Gradstein et al., 2012). The lack of other well-established polarity transitions along both successions precludes any possibility of determining the time span for accumulation of these sediments.

Both columns also show a short interval of reversed polarity near their top (at 137 m in *HN* and at 285 m in *Re*). It is reasonable to assign it to one or both of the short reverse intervals at the base of chron C32 (Fig. 15). However, if the reversed interval present at the top of both columns were C32r.2r, the sedimentation rate would be 0.012 mm/y. Correlation of these short reverse intervals with the base of chron C32 would imply an early Maastrichtian age for the top of the section, which is not consistent with ammonite assemblages in the Rabot Formation. Maastrichtian ammonites only appear in Assemblage 10 (Olivero and Medina, 2000; Olivero, 2012a), at least 700 m stratigraphically above our sections. The fact that the recording of this short reverse interval is very similar in extension and stratigraphic position in both sections, turns unlikely to be an artifact. We interpret that it probably corresponds to 33n.2r or 33n.1r magnetosubzones identified in Beerpaw Shale by Lerbekmo and Braman (2005).

The mean characteristic remanence direction was calculated by combining all the directions from both sections (Fig. 16) and results are summarized in Table 6. Due to the almost horizontal character of the strata, tilt test results indeterminate. Southeastern James

Fig. 17. Upper Cretaceous reference paleopoles of 90 and 60 Ma for the Antarctic Peninsula (Poblete et al., 2011), and paleomagnetic pole of the Rabot Formation (80 Ma, see Table 6). All poles are represented with their respective A95.

Ross Island strata attitude is 20°/10° (right hand rule convention) and, except for local variations that usually do not outgrow the 10° in both strike and dip, this almost horizontal attitude is constant in *HN* and *Re*. This geological setting makes expectable an indeterminate tilt test. Reversal test (McFadden and McElhinny, 1990) is negative between normal and reverse mean directions. Selecting reverse directions obtained from PCA only (Table 6) results in a positive reversal test. However, the large critical angle would label the test as indeterminate for the classification of McFadden and McElhinny (1990).

To calculate the paleomagnetic pole for the Rabot Formation, we used bedding corrected directions obtained from PCA only, as failure of the reversal test when including those obtained from great circle analysis suggest not fully erased secondary magnetizations in these samples. The resultant mean direction is **Dec:** 359.0°, **Inc:** −68.8°, **α95**: 11.8° (Table 6).

Our paleomagnetic pole for the Rabot Formation (80 Ma) and the two Upper Cretaceous/Paleocene reference poles for the Antarctic Peninsula recently computed by Poblete et al. (2011) for 60 Ma and 90 Ma are presented in Fig. 17. The paleopole for the Rabot Formation is consistent within error with both reference poles. This confirms that, within the large uncertainties of the data, no large tectonic rotation affected the northern Antarctic Peninsula since the Late Cretaceous, neither it suffered a large oroclinal bending.

6. Conclusions

A magnetostratigraphic study was carried out along two sections of the Rabot formation exposed in the James Ross Island, Antarctic Peninsula, located some 7 km apart.

Bulk susceptibility values were mostly low, but allowed to define three consecutive subsections or domains in both columns, with the middle one having relatively higher susceptibility values. Section correlation indicates that this pattern of bulk susceptibility values is diachronic. Susceptibility is dominated by paramagnetic minerals and AMS studies show a depositional fabric with low compaction degree, indicating that beds were not significantly buried. *Re* section presents a grouping of *k1* axes in a NE-SW direction (almost perpendicular to the main paleocurrents) that could represent a very weak tectonic overprint developed during the Late Cretaceous inversion of the James Ross Basin.

Detailed stepwise demagnetization of all samples permitted to isolate the characteristic remanence by means of PCA, although great circles had to be used in several cases and many samples showed unstable behavior.

According to rock-magnetic analyses (thermomagnetic curves, Lowrie-Fuller tests and hysteresis cycles) PSD titanomagnetite is the most likely remanence carrier.

Both sections showed a consistent magnetostratigraphy with a lower section of reverse polarity followed by an upper one of normal polarity. Biostratigraphic age constraints suggest that the polarity transition most likely corresponds to C33r/C33n with an age of 79.90 Ma and occur in the middle part of member II of the Rabot Formation.

The presence of one short interval of reverse polarity near the top of both successions probably corresponds to 33n.2r or 33n.1r magnetosubzones identified in Beerpaw Shale by Lerbekmo and Braman (2005).

The computed paleopole is consistent with two Upper Cretaceous paleopoles for Antarctic Peninsula obtained by Poblete et al. (2011), which suggest lack of tectonic rotation or oroclinal bending of this region since the Late Cretaceous.

Acknowledgements

To the Instituto Antártico Argentino for the logistic support during the antarctic field seasons, and the NSF Office of Polar Programs for support of the laboratory work at Caltech. Grants from ANPCyT (PICTO 2010-0114 to E. Olivero) and Universidad de Buenos Aires (UBACyT 20020130100465BA to A. Rapalini) provided additional support for this research. To A. Sobral, D. Smith, M. E. Raffi, S. García, who were very helpful during fieldworks. To the reviewers, whose comments considerably improved the final result.

References

Andersson, J.G., 1906. On the geology of Graham Land. Bulletin of the Geological Institution of the University of Upsala 7, 19–71.
Bibby, J.S., 1966. The stratigraphy of part of north-east Graham Land and the James Ross Island Group. British Antarctic Survey Scientific Reports 53, 1–47.
Buatois, L.A., Lopez Angriman, A.O., 1992. The ichnology of a submarine braided channel complex: the Whisky Bay Formation, Cretaceous of James Ross Island, Antarctica. Palaeogeography Palaeoclimatology Palaeoecology 94, 119–140.
Buatois, L.A., López Angriman, A.O., 1992. Evolución de sistemas deposicionales en el Cretácico del Grupo Gustav, Isla James Ross, Antártida. In: Rinaldi, C.A. (Ed.), Geología de La Isla James Ross. Instituto Antártico Argentino, Buenos Aires, pp. 263–297.
Crame, J.A., Pirrie, D., Riding, J.B., Thomson, M.R.A., 1991. Campanian-Maastrichtian (Cretaceous) stratigraphy of the James Ross Island area, Antarctica. Journal of the Geological Society of London 148, 1125–1140. http://dx.doi.org/10.1144/gsjgs.148.6.1125.
Day, R., Fuller, M., Schmidt, V.A., 1977. Hysteresis properties of titanomagnetites: grain-size and compositional dependence. Physics of the Earth and Planetary Interiors 13, 260–267. http://dx.doi.org/10.1016/0031-9201(77)90108-X.
del Valle, R.A., Fourcade, N.H., Medina, F.A., 1983. Geología del extremo norte del borde oriental de la península antártica e islas adyacentes entre los 63° 25' y los 65° 15' de latitud sur. Dirección Nacional del Antártico, Instituto Antártico Argentino.
Dunlop, D.J., 2002. Theory and application of the Day plot (Mrs/Ms versus Hcr/Hc) 1. Theoretical curves and tests using titanomagnetite data. Journal of Geophysical Research 107, 1–22. http://dx.doi.org/10.1029/2001JB000486.
Ellwood, B.B., Ledbetter, M.T., 1977. Antarctic bottom water fluctuations in the Vema Channel: effects of velocity changes on particle alignment and size. Earth and Planetary Science Letters 35, 189–198. http://dx.doi.org/10.1016/0012-821X(77)90121-2.
Farquharson, G.W., 1984. Late Mesozoic, non-marine conglomeratic sequences of northern Antarctic Peninsula (the Botany Bay Group). British Antarctic Survey Bulletin 65, 1–32.

Feldmann, R.M., Woodburne, M.O., 1988. Geology and paleontology of Seymour island, Antarctic Peninsula. Geological Society of America Memoir 169.
Francis, J.E., Crame, J.A., Pirrie, D., 2016. Cretaceous-Tertiary high-latitude palaeoenvironments, James Ross Basin, Antarctica: introduction. Geological Society London Special Publications 258, 1–5.
Gradstein, F.M., Ogg, J.G., Schmitz, M., Ogg, G. (Eds.), 2012. The geologic time scale 2012. Elsevier.
Hathway, B., Survey, B.A., Cross, H., Road, M., Cb, C., 2000. Continental rift to back-arc basin : Jurassic – Cretaceous stratigraphical and structural evolution of the Larsen Basin, Antarctic Peninsula. Journal of the Geological Society of London 157, 417–432.
Ineson, J.R., 1989. Coarse-grained submarine fan and slope apron deposits in a Cretaceous back-arc basin, Antarctica. Sedimentology 36, 793–819. http://dx.doi.org/10.1111/j.1365-3091.1989.tb01747.x.
Ineson, J.R., Crame, J.A., Thomson, M.R.A., 1986. Lithostratigraphy of the Cretaceous Strata of West James Ross Island, Antarctica. Cretaceous Research 7, 141–159.
Jelinek, V., 1981. Characterization of the magnetic fabric of rocks. Tectonophysics 79, T63–T67.
Johnson, H.P., Lowrie, W., Kent, D.V., 1975. Stability of anhysteretic remanent magnetization in fine and coarse magnetite and maghemite particles. Geophysical Journal International 41, 1–10.
Kirschvink, J.L., 1980. The least-squares line and plane and the analysis of palaeomagnetic data. Geophysical Journal of the Royal Astronomical Society 62, 699–718.
Lerbekmo, J.F., Braman, D.R., 2005. Magnetostratigraphic and palynostratigraphic correlation of late Campanian to early Maastrichtian strata of the Bearpaw and Horseshoe Canyon formations between the CPOG Strathmore corehole and the Red Deer Valley section, Alberta, Canada. Bulletin of Canadian Petroleum Geology 53, 154–164. http://dx.doi.org/10.2113/53.2.154.
Lirio, J.M., Marenssi, S.A., Santillana, S., Marshall, P., 1989. El Grupo Marambio en el Sudeste de la isla James Ross, Antártida. Instituto Antártico Argentino Contribución 371, 1–46.
Lowrie, W., Fuller, M., 1971. On the alternating field demagnetization characteristics of multidomain thermoremanent magnetization in magnetite. Journal of Geophysical Research 76, 6339–6349. http://dx.doi.org/10.1029/JB076i026p06339.
Macellari, C.E., 1988. Stratigraphy, sedimentology, and paleoecology of Upper Cretaceous/Paleocene shelf-deltaic sediments of Seymour Island. Geological Society of America Memoir 169, 25–54.
Macellari, C.E., 1986. Late Campanian-Maastrichtian ammonite fauna from Seymour Island (Antarctic Peninsula). Memoir – Paleontological Society (supplement title) 1–55.
Marenssi, S.A., Lirio, J.M., Santillana, S., Martinioni, D.R., Palamarczuk, S., 1992. El Cretácico Superior del sudeste de la isla James Ross, Antártida. In: Geología de La Isla James Ross. Instituto Antártico Argentino, pp. 77–85.
Marenssi, S.A., Net, L., Santillana, S., 2002. Provenance, environmental and paleogeographic controls on sandstone composition in an incised-valley system: the Eocene La Meseta Formation, Seymour Island, Antarctica. Sedimentary Geology 150, 301–321.
Martinioni, D.R., Rinaldi, C.A., 1992. La Formación Rabot (Cretácico superior, Isla James Ross, Antártida): Un ciclo transgresivo-regresivo de plataforma con dominio de procesos de tormenta. In: Geología de La Isla James Ross, Antártida. Instituto Antártico Argentino, Buenos Aires, pp. 101–123.
Mattei, M., Sagnotti, L., Faccenna, C., Funiciello, R., 1997. Magnetic fabric of weakly deformed clay-rich sediments in the Italian peninsula: relationship with compressional and extensional tectonics. Tectonophysics 271, 107–122. http://dx.doi.org/10.1016/S0040-1951(96)00244-2.
McFadden, P.L.L., McElhinny, M.W.W., 1990. Classification of the reversal test in palaeomagnetism. Geophysical Journal International 103, 725–729.
McFadden, P.L.L., McElhinny, M.W.W., 1988. The combined analysis of remagnetization circles and direct observations in palaeomagnetism. Earth and Planetary Science Letters 87, 161–172. http://dx.doi.org/10.1016/0012-821X(88)90072-6.
Medina, F.A., Scasso, R.A., del Valle, R.A., Olivero, E.B., Malagnino, E.C., Rinaldi, C.A., 1989. Cuenca mesozoica del margen nororiental de la península Antártica, Cuencas Sedimentarias Argentinas. Instituto Superior de Correlación Geológica, Serie Correlación Geológica.
Milanese, F.N., Kirschvink, J.L., Olivero, E.B., Rapalini, A.E., 2013. Magnetostratigraphy of an Upper Cretaceous Section of James Ross Basin, Antarctica. Latinmag Letters 3, 1–9.
Montgomery, P., Hailwood, E.A., Gale, A.S., Burnett, J.A., 1998. The magnetostratigraphy of Coniacian-Late Campanian chalk sequences in southern England. Earth and Planetary Science Letters 156, 209–224. http://dx.doi.org/10.1016/S0012-821X(98)00008-9.
Olivero, E.B., 2012a. Sedimentary cycles, ammonite diversity and palaeoenvironmental changes in the Upper Cretaceous Marambio Group, Antarctica. Cretaceous Research 34, 348–366. http://dx.doi.org/10.1016/j.cretres.2011.11.015.
Olivero, E.B., 2012b. New Campanian kossmaticeratid ammonites from the James Ross Basin, Antarctica, and their possible relationships with Jimboiceras? antarcticum Riccardi. Revue de Paleobiologie 31, 133–149.
Olivero, E.B., 1992. Asociaciones de Amonites de la Formación Santa Marta (Cretácico Tardío), Isla James Ross, Antártida. In: Rinaldi, C.A. (Ed.), Geología de La Isla James Ross. Instituto Antártico Argentino, Buenos Aires, pp. 45–75.
Olivero, E.B., Medina, F.A., 2000. Patterns of Late Cretaceous ammonite biogeography in southern high latitudes: the family Kossmaticeratidae in Antarctica. Cretaceous Research 21, 269–279. http://dx.doi.org/10.1006/cres.1999.0192.
Olivero, E.B., Mussel, F.A., 1993. Biofacies de Inoceramus (Bivalvia) en ambientes marinos proximales del Cretácico superior de Antártida. In: 2das. Jornadas Sobre Investigaciones Antárticas. Instituto Antártico Argentino-INGEIS, Buenos Aires, pp. 189–190.
Olivero, E.B., Ponce, J.J., Martinioni, D.R., 2008. Sedimentology and architecture of sharp-based tidal sandstones in the upper Marambio Group, Maastrichtian of Antarctica. Sedimentary Geology 210, 11–26. http://dx.doi.org/10.1016/j.sedgeo.2008.07.003.
Olivero, E.B., Scasso, R.A., Rinaldi, C.A., 1986. Revision of the Marambio Group, James Ross Island, Antarctica. Instituto Antártico Argentino Contribución 331, 1–30.
Palamarczuk, S., 1993. Bioestratigrafía de dinoflagelados del Cretácico superior en las islas James Ross y Vega, Antártida. Segundas Jornadas de Comunicaciones sobre Investigaciones Antárticas. Instituto Antártico Argentino, Buenos Aires, pp. 191–192.
Pan, Y., Zhu, R., Banerjee, S.K., Gill, J., Williams, Q., 2000. Rock magnetic properties related to thermal treatment of siderite: behavior and interpretation. Journal of Geophysical Research 105, 783–794. http://dx.doi.org/10.1029/1999JB900358.
Pirrie, D., 1989. Shallow marine sedimentation within an active margin basin, James Ross Island, Antarctica. Sedimentary Geology 63, 61–82.
Pirrie, D., Crame, J.A., Riding, J.B., Lomas, S.A., Riding, J.B., 1997. Late Cretaceous stratigraphy of the Admiralty Sound region, James Ross Basin, Antarctica. Cretaceous Research 18, 109–137. http://dx.doi.org/10.1016/0195-6671(91)90036-C.
Poblete, F., Arriagada, C., Roperch, P., Astudillo, N., Hervé, F., Kraus, S., Le Roux, J.P., 2011. Paleomagnetism and tectonics of the South Shetland Islands and the northern Antarctic Peninsula. Earth and Planetary Science Letters 302, 299–313.
Reguero, M., Goin, F., Hospitaleche, C.A., Marenssi, S.A., Dutra, T., 2013. Late Cretaceous/Paleogene West Antarctica Terrestrial Biota and its Intercontinental Affinities. In: Springer Briefs in Earth System Sciences, pp. 19–25. http://dx.doi.org/10.1007/978-94-007-5491-1_1.
Riding, J.B., Crame, J.A., Dettmann, M.E., Cantrill, D.J., 1998. The age of the base of the Gustav Group in the James Ross Basin, Antarctica. Cretaceous Research 19, 87–105. http://dx.doi.org/10.1006/cres.1998.0098.
Rinaldi, C.A., Massabie, A., Morelli, J., Rosenman, H.L., del Valle, R.A., 1978. Geología de la isla Vicecomodoro Marambio. Contribución del Instituto Antártico Argentino 217, 1–37.
Roberts, A.P., 1995. Magnetic properties of sedimentary greigite (Fe3S4). Earth and Planetary Science Letters 134, 227–236.
Sagnotti, L., Winkler, A., Montone, P., Di Bella, L., Florindo, F., Mariucci, M.T., Marra, F., Alfonsi, L., Frepoli, A., 1999. Magnetic anisotropy of Plio-Pleistocene sediments from the Adriatic margin of the northern Apennines (Italy): implications for the time-space evolution of the stress field. Tectonophysics 311, 5041181. http://dx.doi.org/10.1016/S0040-1951(99)00159-6.
Snowball, I.F., 1997. The detection of single-domain greigite (Fe3S4) using rotational remanent magnetization (RRM) and the effective gyro field (Bg): mineral magnetic and palaeomagnetic applications. Geophysical Journal International 130, 704–716. http://dx.doi.org/10.1111/j.1365-246X.1997.tb01865.x.
Suzuki, Y., Kopp, R.E., Kogure, T., Suga, A., Takai, K., Tsuchida, S., Ozaki, N., Endo, K., Hashimoto, J., Kato, Y., Mizota, C., Hirata, T., Chiba, H., Nealson, K.H., Horikoshi, K., Kirschvink, J.L., 2006. Sclerite formation in the hydrothermal-vent "scaly-foot" gastropod – Possible control of iron sulfide biomineralization by the animal. Earth and Planetary Science Letters 242, 39–50. http://dx.doi.org/10.1016/j.epsl.2005.11.029.
Tobin, T.S., Ward, P.D., Steig, E.J., Olivero, E.B., Hilburn, I.A., Mitchell, R.N., Diamond, M.R., Raub, T.D., Kirschvink, J.L., 2012. Extinction patterns, δ 18 O trends, and magnetostratigraphy from a southern high-latitude Cretaceous–Paleogene section: links with Deccan volcanism. Palaeogeography Palaeoclimatology Palaeoecology 350–352, 180–188. http://dx.doi.org/10.1016/j.palaeo.2012.06.029.
Whitham, A.G., 1993. Facies and depositional processes in an Upper Jurassic to Lower Cretaceous pelagic sedimentary sequence, Antarctica. Sedimentology 40, 331–349.
Whitham, A.G., Ineson, J.R., Pirrie, D., 2006. Marine volcaniclastics of the Hidden Lake Formation (Coniacian) of James Ross Island, Antarctica: an enigmatic element in the history of a back-arc basin. Geological Society London, Special Publications 258, 21–47.
Zijderveld, J.D.A., 1967. AC demagnetization of rocks: analysis of results. Methods in Paleomgnetism 254–286.

Appendix A. Supplementary data

Supplementary data related to this article can be found at http://dx.doi.org/10.1016/j.cretres.2016.12.016.